Received: 15 June 2021 | Revised: 8 October 2021 | Accepted: 16 November 2021

DOI: 10.1002/pts.2624

Packaging Technology and Science
An International Journal

WILEY

RESEARCH ARTICLE

# Design of glass containers for submarine carbon storage

Cheng Fu | Nicola Cefis | Massimiliano Cremonesi | Umberto Perego | Stefano Caserini | Mario Grosso

Department of Civil and Environmental Engineering, Politecnico di Milano, Milan, Italy

**Correspondence**
Cheng Fu, Department of Civil and Environmental Engineering, Politecnico di Milano, Piazza Leonardo da Vinci 32, 20133 Milan, Italy.
Email: cheng.fu@polimi.it

**Funding information**
Amundi SGR SpA; Politecnico di Milano

This work deals with the preliminary design of glass containers to be deposited on the seabed at 2000 m depth after being filled with liquefied carbon dioxide ($CO_2$) at a pressure of 10 MPa. The specific purpose is to provide preliminary structural analyses of the containers to be employed in a novel patent $CO_2$ storage method called confined submarine carbon storage (CSCS). The core steps of the CSCS technology are the container manufacturing and filling with high-pressure liquid $CO_2$. Consequently, the container geometry, material properties and structural response are the most critical aspects in the container design. Due to the low cost and to the high stability in salty environment, glass has been identified as a suitable material for the CSCS technology. Furthermore, the high compressive resistance allows glass containers to be deposited on the seabed where the external water pressure exceeds the internal pressure of liquefied carbon dioxide. On the other hand, the limited tensile resistance of glass requires a careful shape design. The glass containers have to be designed to withstand stresses generated during their entire working life. This includes $CO_2$ filling, the launching, the impact with the seabed and the final piling up and stacking of a huge number of containers. Finite element analyses have been performed in order to define the container shape, conjugating an acceptable storage capacity with a safe mechanical response during both the filling and deposition phases.

**KEYWORDS**
borosilicate glass, confined submarine carbon storage, finite element analysis, thin shells

## 1 | INTRODUCTION

The ambitious objective of the Paris Agreement, to limit global warming well below 2°C with respect to the pre-industrial levels (and make efforts to limit it below 1.5°C), requires a rapid decrease in greenhouse gas emissions and the removal of large quantities of $CO_2$ from the atmosphere.[1–3] Among climate mitigation technologies, proposed to reduce the anthropogenic $CO_2$ release into the atmosphere, carbon capture and storage (CCS) has been extensively studied in the last 30 years. CCS consists of the separation of $CO_2$ from flue gas produced in power stations or other industrial sources and its subsequent permanent storage. Several capture technologies have been developed, and they are already at a commercial level. Furthermore, different storage methods have been proposed (e.g., geological storage is at the highest levels of development).

Since the publication of the Intergovernmental Panel on Climate Change (IPCC) Special Report on Carbon Capture and Storage,[4] CCS has developed at a slow pace.[5] Although there have been

technological progresses, more incisive actions are needed to accelerate its development.[6] Even if CCS is ready for large-scale deployment, the problems related to the overall cost, the storage risks and the negative public perception[7] in many places have severely hindered the growth pace of the technology. Today, there are 28 CCS facilities in operation, with about 40 Mt/year of $CO_2$ stored, mainly through enhanced oil recovery.[8]

While the capture is the most expensive phase, storage is the most critical for different reasons. Although the theoretical storage potential is enormous, the effective storage capacity available has severe limitations in many regions.[9] Furthermore, a long time (from 5 to 10 years) is required to thoroughly assess a new saline formation potentially suitable for $CO_2$ storage, even when theoretical estimates are already available and look promising, and this requires a large upfront investment.[10] Another critical point is that the geographical distribution of the storage locations is uneven and there is need to concentrate $CO_2$ emissions sources in large clusters to minimize the logistic costs.[11] These limitations have raised doubts on the real capability of geological CCS to cope with the multi-Gton/year $CO_2$ storage needs in the next decades.[12] The availability of alternative ways to permanently sequester large quantities of $CO_2$ is of a great interest for CCS deployment.

A new form of carbon storage, called confined submarine carbon storage (CSCS), has been discussed by Caserini et al.[13] The basic concept of the CSCS is to store the captured $CO_2$ in a compressed liquid form inside glass containers and transport them through offshore pipelines into the ocean. The proposed CSCS system is composed of different facilities: a furnace for the manufacturing of the glass containers, a station for filling and sealing each container, a launcher and the launching pipe. Through the launching tube, containers are transported from the land to the bottom of the sea at a depth typically between 1000 and 2000 m, where the hydrostatic pressure exceeds the internal pressure of the $CO_2$. Caserini et al[13] assessed through a life cycle assessment (LCA) and with a preliminary risk assessment and cost analysis the environmental and economic benefits and cost of the CSCS technology. Moreover, Barreto et al[14] analysed the potential application of the CSCS for cement plants in different geographical and economic contexts. To further understand the role of CSCS technology as a long-term $CO_2$ storage solution, there is the need of a detailed assessment of the main design parameters.

The choice of structural materials for the geological storage of liquefied carbon dioxide must cover both mechanical considerations (bearing capacity of the container) and evaluations of performance in terms of durability and chemical–physical resistance. These considerations are closely linked to each other and to the physical structure of the material.

Structural materials are commonly divided into metals, ceramics, polymers and composites.[15] Each of the first three categories is characterized by specific physical peculiarities that determine the structural, chemical and physical properties exhibited macroscopically, while the last category consists of the composition of different materials belonging to two or three of the main categories.

Metallic materials are widely used in structural applications due to the high resistance and ductility that characterize their behaviour, but in moderate and aggressive environment, they show poor performance in terms of durability. Polymeric materials can degrade by breaking the inter-chain and intra-chain bonds with consequent structural damage and diffusion of microplastics in the environment.

The materials that are most suitable for the geological deposit are ceramics. This class of amorphous solids is composed by metallic and non-metallic elements joined by ionic or covalent bonds. From the chemical–physical and structural point of view, materials belonging to this class are characterized by high hardness, low electrical and thermal expansion coefficients, and high resistance to chemical damage induced by solvents and saline solutions. The excellent chemical–physical resistance has led glass to be the material of choice for the geological storage of highly active radioactive waste.[16,17] A strongly negative aspect that concerns almost all ceramic materials is the low toughness and brittle failure behaviour.[18] Glass, both for its macroscopic physical behaviour and for the type of chemical bonds, can be considered a ceramic material. In reality, glass should be considered a liquid material characterized by such a high viscosity to allow it to be considered, for temperature ranges far from the melting point and for non-geological observation times, as a solid.[19] Furthermore, the chemical–physical resistance and solid-like behaviour of glass have been widely documented through the analysis of millenarian archaeological remains (bow arrows, containers and jewels) perfectly preserved up to the present day.[20]

The type of glass most commonly used in industrial applications is silico–soda–lime glass, characterized by short-range order and formed by a mesh of silicon oxides modified by the presence of $Na^+$ and $Ca^{2+}$ ions. For the considered application, the use of borosilicate glasses has been preferred, instead of the classic silico–soda–lime glass, because they are characterized by a greater chemical resistance to aqueous solutions and by a lower coefficient of thermal expansion. This type of glass is obtained by the addition of boron, in order to form networks consisting of silicon oxides and boron oxides. Alkaline ions ($Na^+$) are always added to bring the coordination of boron to 4, thus also increasing the material viscosity. For this reason, borosilicate glass is the material of selection in many contexts with high chemical and physical aggressiveness such as glassworks in the pharmaceutical and chemical industries.

In this work, mechanical and geometrical features of the glass CSCS container are discussed. Finite element analyses and a topological optimization process are carried out with the commercial software ABAQUS/CAE, focusing on the safety checks. After defining the final shape, the quantity of required glass for manufacturing and its storage capacity have been identified. Stresses generated by pressures during the most severe filling conditions have been recomputed through FEM. Furthermore, the container falling velocity in the steady state and stresses generated by pressures at the storage site have been evaluated. Finally, 3D explicit dynamics analyses have been performed by ABAQUS/CAE, focusing on principal stresses caused by the impact of the container against the seabed and against a stored container.

The paper is structured as follows. In Section 2, the CSCS process, the adopted material and the preliminary shape of the container are introduced. Section 3 describes the topological optimization of the container, while Section 4 discusses the sinking speed and stress analyses at 2000 m depth considering the acting pressures and impact against the seabed. Moreover, the dependency on the geometrical parameters is highlighted. Finally, conclusions are addressed in Section 5.

## 2 | PROCESS DESCRIPTION

### 2.1 | Containers for submarine carbon storage process

This study analyses the containers of the liquefied carbon dioxide of the confined submarine carbon storage (CSCS) process proposed by Caserini et al.[13] The CSCS system, depicted in Figure 1, consists of a plant chain that starts from the collection of carbon dioxide resulting from industrial processes up to the deposition in sealed containers on the seabed through the following phases:

① a system for the liquefaction of carbon dioxide resulting from production processes is installed at the industrial site;

② a plant for the melting of glass and the construction of the containers is built near the industrial site;

③ the liquefied carbon dioxide and the containers are sent to the storage and launch facility;

④ in the storage plant, the containers are filled with pressurized liquid carbon dioxide and with sand to control the sinking speed; and

⑤ the filled and sealed containers are sent to the launch pipe for sinking using as carrier the seawater taken by the suction pipe.

The conceptual model is suitable for storing the carbon dioxide produced by industrial plants located in maritime areas, and the modularity of the same allows for the application to both small and large plants.

This study presents the structural optimization of the containers, starting from the pressure chamber hosting them during the $CO_2$ filling process up to the sinking and impact against the sea bottom. At the first stage, to balance the $CO_2$ pressure in the container, the chamber is internally pressurized with water at $P = 10$ MPa. The chamber has two valves: an inlet valve to fill the empty container (at ambient pressure) and an outlet valve (at the imposed working pressure) for the discharge of the filled container (see Figure 2). In this phase, it is essential to close hermetically the chamber from the external environment.

After the filling procedure, the container is sealed through a welding operation, sealing the plug to the body. The container is then discharged from the chamber and transported to the storage site by pipelines. Once the containers are filled up, they should be always subjected to an external pressure equal or greater than the internal one exerted by the liquefied carbon dioxide. Therefore, transportation ducts have to be pressurized internally to balance the $CO_2$ pressure in the container. The pipeline system is deployed following the seabed profile. Since irregular morphology with varying slopes is expected,

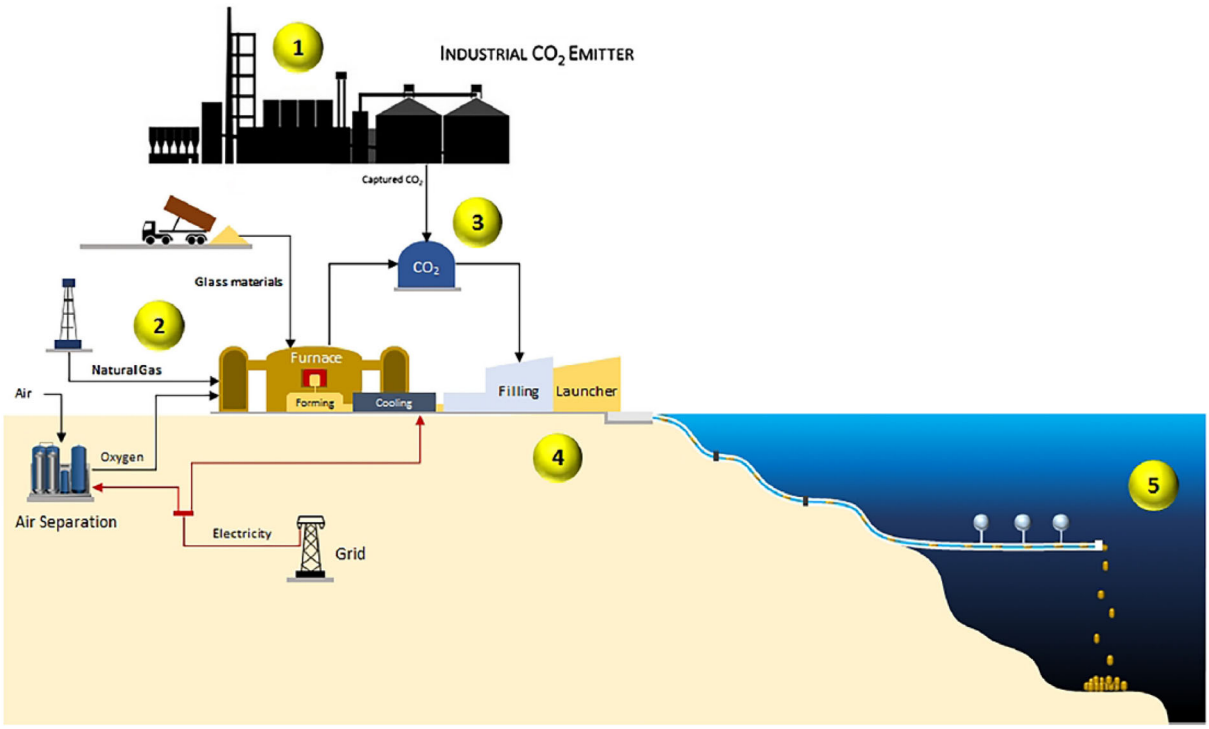


**FIGURE 1** Scheme of the CSCS process (from Caserini et al.[13]). (1) The emitter implements the $CO_2$ capture system. (2) Production of glass containers. (3) $CO_2$ collected from emitter and from containers production. (4) Containers filling and launching. (5) Filled containers are transported and released

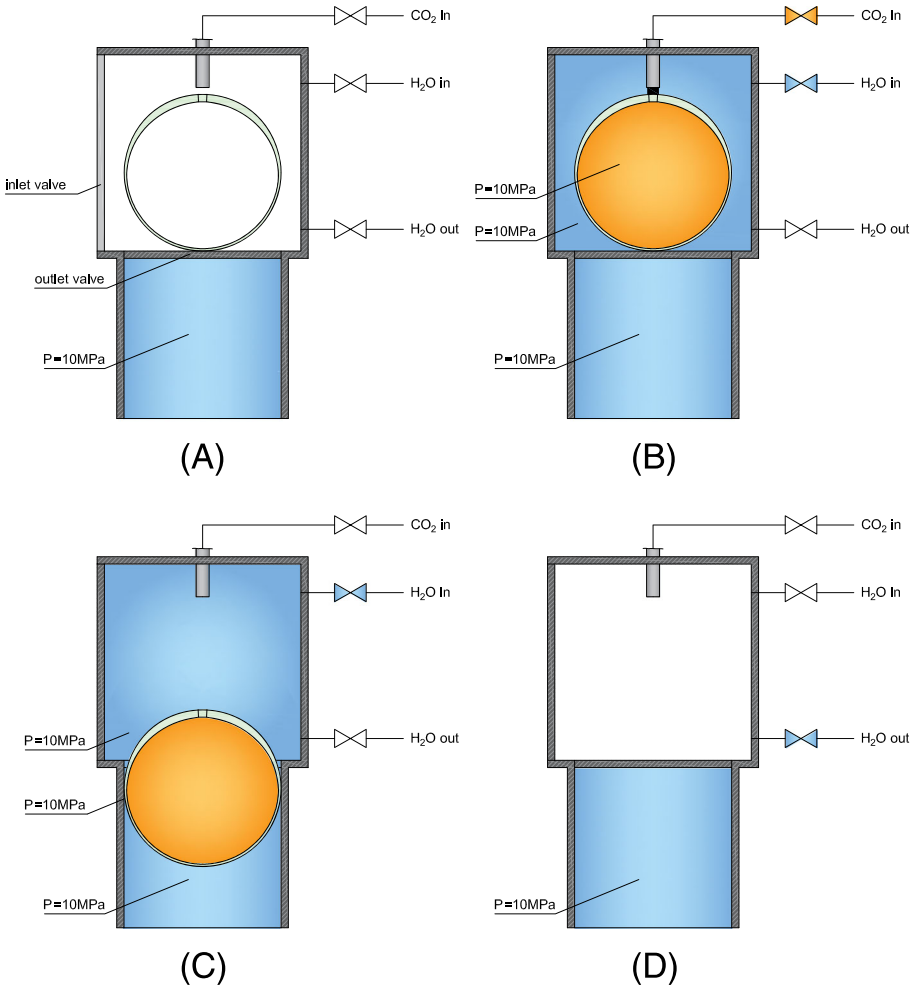


**FIGURE 2** Container filling process. (A) Load the empty container into the chamber at ambient pressure through the inlet valve, and close hermetically the chamber from external environment. (B) Increase the pressure inside the chamber up to the predefined working pressure, fill up the container with $CO_2$ and seal the full container by welding. (C) Open the outlet valve to release the filled container into the pipeline at the working pressure. (D) Close the outlet valve, and empty the chamber to perform a new cycle

propulsive force is required to transport the containers along the duct with controlled velocity. When the container is released from the chamber, the pressurized water can be emptied and a new cycle of chamber pressurization, container filling and welding can take place. The main phases are schematically shown in Figure 2.

## 2.2 | Material

Glass has been assumed as a suitable material for the CSCS containers to be used in the marine environment, since the chosen material should be able to resist salt corrosion as well as water pressure in deep sea. Furthermore, glass allows to optimize the durability and resistance of the containers and to reduce the energy consumption and economic costs for the supply of raw materials. Borosilicate glass has been identified as an efficient material to contain liquid $CO_2$ since it has a high mechanical (in compression), thermal and chemical resistance. Glass is considered as a homogenous and isotropic material characterized by an amorphous structure and with a mechanical response that can be considered linear elastic up to failure. While an excellent compression resistance can be observed, the bearing capacity of glass in tension is very limited due to the presence of defects, which make it brittle. The failure of glass is strongly influenced by size effects and loading duration. The level of tension should be kept as low as possible since a small value is enough to propagate a crack. Together with other initial defects, residual stresses are always present in glass due to non-uniform cooling process. A common technique used to remove these residual stresses consists of a thermal treatment, whereby the material is annealed at the end of the production,[21] with consequent removal of self-stresses. In this phase, the glass container is let cooling down slowly. In the present work, residual stresses due to the production process are not considered since an annealing treatment is assumed to have been applied to the glass container at the end of the production process.

The analysis of the glass mechanical response used in the production of the containers, to be adopted for CSCS, has been carried out in compliance with the international standards EN 1748-1-1.[22] The mechanical parameters used in the analyses are shown in Table 1, where $E$ is Young's modulus, $\nu$ is Poisson's ratio, $\rho$ is the density, and $f_{g,k}$ and $f_{c,k}$ are the characteristic strengths in tension and compression, respectively.

The values of the design strength in tension $f_{g,d}$ and compression $f_{c,d}$ are obtained through a reduction of characteristic values by

**TABLE 1** Borosilicate material properties[22]

| $E$ (MPa) | $\nu$ (—) | $\rho$ (kg/m$^3$) | $f_{g,k}$ (MPa) | $f_{c,k}$ (MPa) |
|---|---|---|---|---|
| 64 000 | 0.20 | 2200 | 45 | 1100 |

resorting to the relationships proposed in CNR-DT 210[23] provided by the Italian National Research Council.

$$f_{g,d} = \frac{f_{g,k} \cdot k_{mod} \cdot k_{ed} \cdot k_{sf} \cdot \lambda_{gA} \cdot \lambda_{gl}}{R_M \gamma_M} = 2.02\text{MPa}$$

$$f_{c,d} = \frac{f_{c,k}}{R_M \gamma_M} = 440\text{MPa}$$

where $k_{mod} = 0.2$ is the reduction coefficient for long-term loads (5000 years), $k_{ed} = 1.0$ is the tension correction factor, $k_{sf} = 0.75$ is the correction factor dependent on the surface profile, $\lambda_{gA} = 0.75$ is the scale factor, $\lambda_{gl} = 1.0$ is the scale boundary factor, $R_M = 1.0$ is the coupled tension-bending factor and $\gamma_M = 2.5$ is the safety factor.

This method for computing the design resistance is consistent with the methodology proposed in European Standard EN 16612:2019 for glass panels with minor variations on the coefficients.

Admissible stress states are assumed to obey the Galileo–Rankine–Navier failure criterion in terms of principal stresses:

$$\sigma^{max}_{max\_prin} < f_{g,d} \quad (1)$$

$$|\sigma^{min}_{min\_prin}| < f_{c,d} \quad (2)$$

## 2.3 | Container structure

To reduce tensile stress states, besides material properties, one important aspect is represented by the container shape. The most convenient typologies for fluid storage rely on thin shell structures for their efficiency and reduced costs.

A capsule-shaped container of dimension 600 × 300 mm has been tentatively assumed by Caserini et al.[13] It is composed of two semi-spherical shells at the ends and of a cylindrical central part. However, from a structural point of view, the mechanical strength of the container is optimized by the spherical shape.

In the present work, a thin spherical vessel of diameter $D = 500$ mm and thickness $t = 3.5$ mm has been taken as a reference container, since it allows for a smaller thickness and consequently for the use of less material. During the $CO_2$ filling process, a borosilicate glass plug is required (see Figure 3). Since the geometry of the plug differs from that of the rest of the container, it represents a disturbance to the membrane behaviour of the container wall, influencing significantly the structural response and requiring a thickness increase to withstand the additional stress. These flexural disturbances occur in a limited portion of the container, and they vanish at a certain distance from the plug. In the remaining regions, the membrane behaviour is recovered.[24,25] This allows to increase the thickness only in the plug region with a connecting region, characterized by a gradual thickness increment, joining the plug and thin shell smoothly (Figure 3).

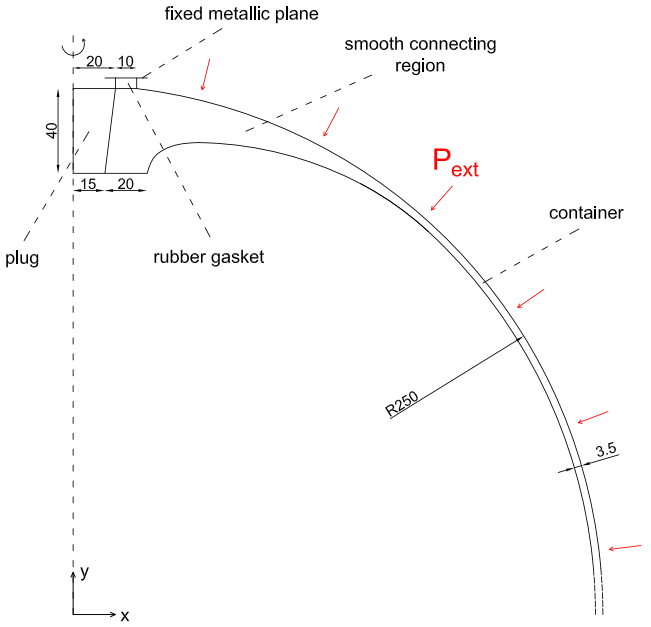


**FIGURE 3** Preliminary container shape (only one quarter of the section is depicted). Values in mm

# 3 | GLASS CONTAINER SHAPE

## 3.1 | Preliminary shape

During the filling phase, the container is kept in a metallic chamber in which an external water pressure $P_{ext} = 10$ MPa is artificially imposed to equilibrate the internal pressure $P_{int} = 10$ MPa. Nevertheless, to account for possible accidents during the filling phase, the container shape design is based on the most severe condition, according to which only the external water pressure of 10 MPa is applied; hence, the balancing effect provided by $CO_2$ is neglected.

In the preliminary model, the shape and dimension of the plug, as well as the container thickness enlargement, have been qualitatively introduced. A static axial symmetric finite element analysis with ABAQUS/CAE has been performed to estimate the stresses generated in the worst loading condition during the filling process by considering the external pressure only. The model is composed by four parts: glass container body, glass plug, rubber gasket and metallic chamber. The latter, due to its high stiffness compared to the other components, is kept fixed and modelled as a rigid plane. The scheme is depicted in Figure 3, while modelling input data are reported in Table 2 where $D_{10}$ and $C_1$ are the new-Hookean strain energy potential parameters used for the rubber gasket. The adopted finite element mesh is constituted by 0.5 mm quadrilateral finite elements with

**TABLE 2** Finite element modelling input data in the preliminary-shaped container

| Component | Number of used elements | Type of used elements | Material | Modelling technique | Modelling parameters |
|---|---|---|---|---|---|
| Plug | 2835 | 8-node biquadratic axisymmetric quadrilateral (CAX8) | Borosilicate glass | Linear elastic homogeneous isotropic | $E = 64000$ MPa $\nu = 0.20$ |
| Container | 21 691 | | | | |
| Gasket | 100 | 8-node biquadratic axisymmetric quadrilateral, hybrid, linear pressure (CAX8H) | Rubber | Hyperelastic with new-Hookean strain energy potential | $D_{10} = 2.5$ MPa $C_1 = 0$ |
| Metallic plane | — | 2-node linear axisymmetric rigid link (RAX2) | Steel | Discrete rigid | — |

**TABLE 3** Adopted friction coefficients

| Material | Friction coefficient |
|---|---|
| Glass–glass | 0.94 |
| Glass–rubber | 0.20 |
| Steel–rubber | 0.80 |

approximately seven elements along the container wall with constant thickness. Surface-to-surface interaction has been adopted between surfaces of the parts with both hard normal and tangential interaction, the latter based on the Mohr–Coulomb approach. The used friction coefficients are reported in Table 3.

The minimum and maximum principal stresses resulting from the axial symmetric finite element analysis (see Figure 4) have been compared to the admissible design stresses. It can be observed that the highest maximum principal stress is larger than the admissible one:

$$\sigma^{max}_{max\_prin} = 22.38\text{MPa} > f_{g,d} = 2.02\text{MPa}$$

Since the external pressure $P_{ext}$ causes overly high level of stress in the preliminary shape, a more appropriate shape must be identified through an optimization process, trying to satisfy the safety check and to achieve a minimum material usage.

## 3.2 | Shape optimization

From the results of the finite element analysis, high values of the principal stresses are obtained at the internal profile of the preliminary shaped container, with the maximum value of tensile stress localized in correspondence of the plug. A topological optimization has been performed using ABAQUS/CAE topological optimization feature, aiming to modify the internal profile and to achieve a more effective shape.[26] This process has been performed by minimizing the strain energy of the system while constraining its volume to 85% of the initial value. Furthermore, a thickness constraint has been introduced in order to keep its value to be larger than 3.5 mm during the entire optimization procedure. An iterative process has been carried out by the software until the imposed conditions have been satisfied. As a result, the container is less material demanding and structurally more efficient.

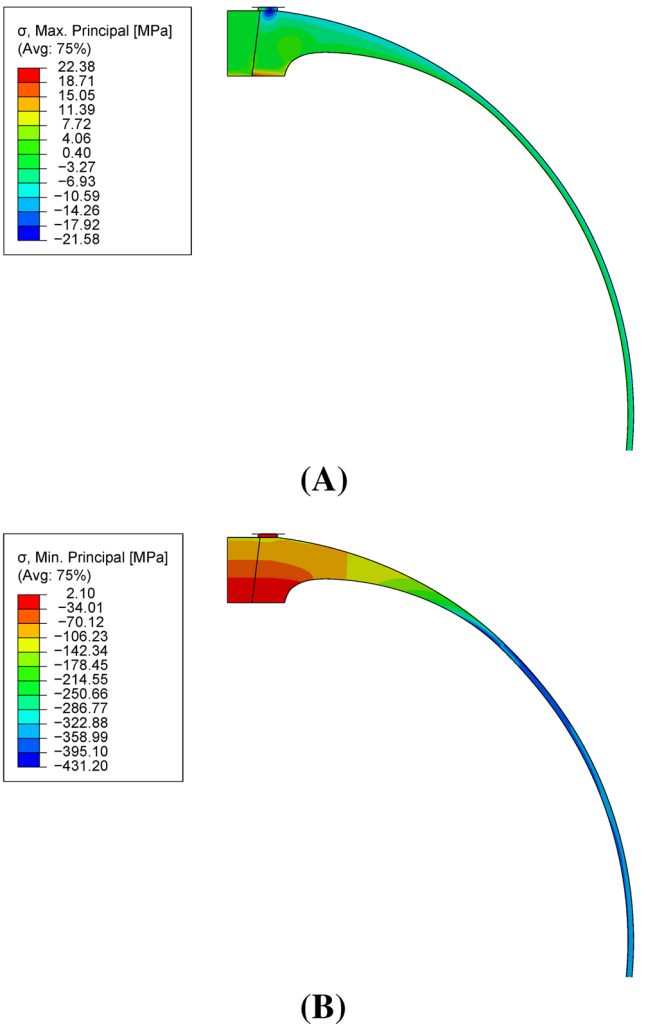


**FIGURE 4** Principal stresses in the preliminary shaped container estimated by axial symmetric finite element analysis. (A) Maximum principal stresses. (B) Minimum principal stresses. Only one quarter of the container section is shown

During the optimization process, the most severe loading condition has been considered by applying the external pressure only. The region to be optimized is represented by the upper part of the container, constituted by the connecting region and by the plug. A simplified model has been set up by merging the plug and the sphere together, as they are made of the same material. Moreover, for the sake of simplicity, both the gasket and the metallic plate have been removed. Their structural contribution has been approximated by a zero vertical displacement (*y* direction; see Figure 3) of the top flat edge. In the reshaping phase, the upper portion will be modified according to the imposed conditions, with no changes occurring in the remaining part. The removed region can be easily visualized since it has been assigned a very low value of relative density by the software (blue region in Figure 5). This fraction, being composed by soft elements, does not contribute to the stiffness of the system. In contrast, hard elements (red region in Figure 5) that have been conserved present a unitary value of relative density.

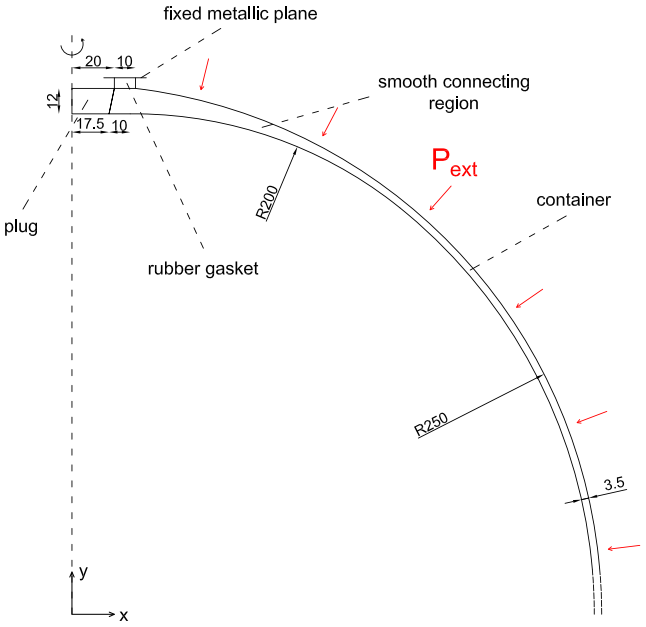


**FIGURE 6** Container shape after topological optimization (only one quarter of the section is depicted). Values in mm

## 3.3 | Optimized shape

A more effective shape, stiffer and less material demanding, has been obtained from the optimization process. While the internal geometric features have been redefined in the upper part of the container, the thickness and the radius have remained unchanged in the other regions. The thickness of the plug has been reduced from 40 to 12 mm after the optimization. The scheme of the optimized container is shown in Figure 6.

The axisymmetric finite element analysis has been carried out again, considering the optimized shape under the most severe loading condition in the filling phase. The same type and average dimension of finite elements have been adopted. The new model accounts for 10 176 and 620 finite elements in the container body and in the plug, respectively. Minimum and maximum principal stresses in the plug and in the container have been estimated (see Figure 7). Far from the enlarged region, constant values of stresses have been obtained as

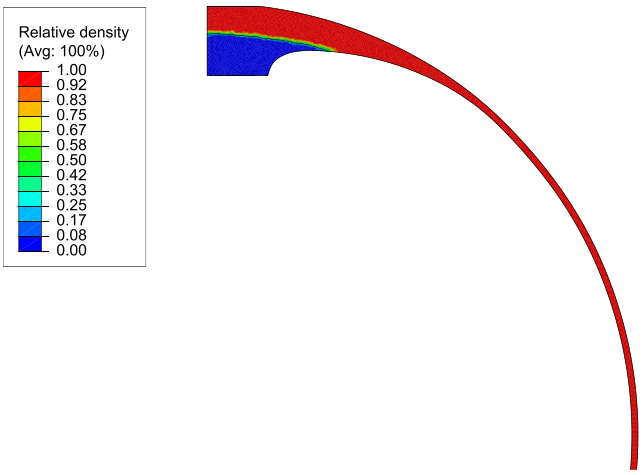


**FIGURE 5** Relative density after topological optimization

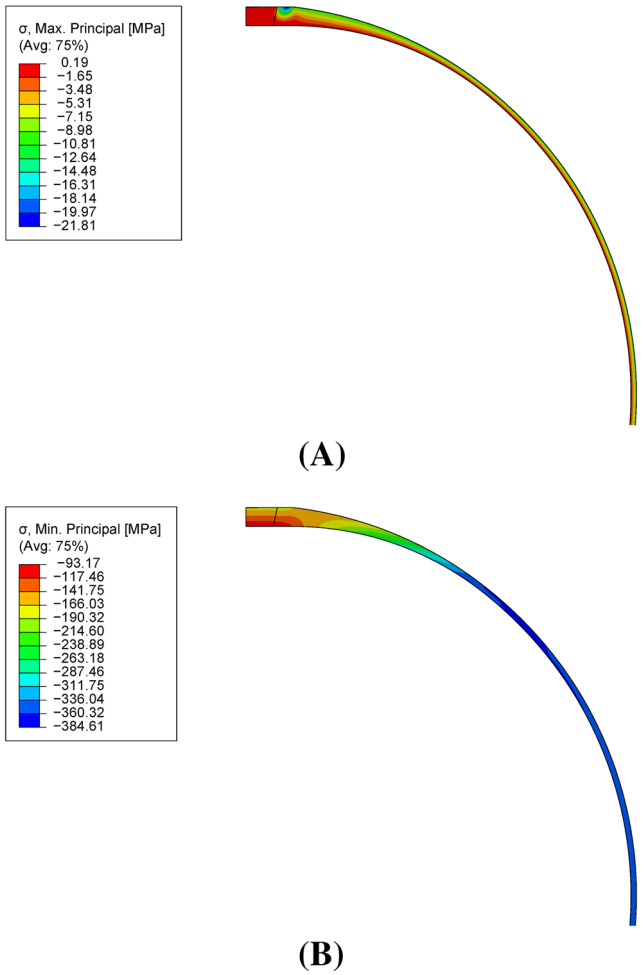


**FIGURE 7** Principal stresses in the optimized container. (A) Maximum principal stresses. (B) Minimum principal stresses. Only one quarter of the container section is shown

the membrane behaviour is recovered. Furthermore, the highest values of principal stresses are everywhere lower than the admissible ones both in tension and in compression:

$$\sigma^{max}_{max\_prin} = 0.19\,\text{MPa} < f_{g,d} = 2.02\,\text{MPa}$$
$$|\sigma^{min}_{min\_prin}| = 384.61\,\text{MPa} < f_{c,d} = 440\,\text{MPa}$$

Hence, the shape and dimensions obtained from the optimization process are verified in terms of bearing capacity.

## 4 | CONTAINER DEPOSITION ON SEA BOTTOM

### 4.1 | Terminal velocity

According to the CSCS technology, once the $CO_2$ filling process is accomplished, glass containers are supposed to be stored on seabed. To do that, a pipeline system launches the containers under water to a distance within 200 km offshore.[13] Once the suitable distance from the coast is reached, the containers are released from the pipeline and start to sink until they deposit onto the storage site. During the falling process, it is essential to ensure that the filled container self-weight overcomes the drag and buoyancy opposing the container drop. The terminal velocity at the time of the impact against the sea bottom can be computed by imposing a zero resultant of the forces acting on the container during the falling motion.

The self-weight $F_p$ of the glass container and of the contained liquefied $CO_2$ can be obtained by multiplying their mass by the gravity acceleration $g$. The uplift buoyancy force $F_b$ is evaluated as the weight of the volume of water corresponding to the container volume. Material density $\rho$ and volume $V$ are reported in Table 4. Subscripts $g$, $CO_2$ and $w$ stand for glass, carbon dioxide and seawater, respectively.

$$F_p = (\rho_g V_g + \rho_{CO_2} V_{CO_2})g = 665.79\,\text{N}$$
$$F_b = \rho_w (V_g + V_{CO_2})g = \rho_w V_w g = 627.26\,\text{N}$$

Since the obtained self-weight of the system is not enough to achieve a downward motion, due to the buoyancy force, additional mass is required to regulate the sinking speed of the sphere. To this purpose, a certain amount of sand has been added to the container, in view of its low cost and large availability. To avoid an excessive reduction of the container $CO_2$ storage capacity, the minimum amount of sand $m_{sand} = 6.76\,\text{kg}$ has been introduced, where the density of sand has been taken equal to that of glass. The resulting mass of glass $m_g$ and mass of liquefied carbon dioxide $m_{CO_2}$ are 6.36 and 54.76 kg, respectively, with a ratio of 11.61%.

Still water has been assumed in deep sea, neglecting the effects of sea currents. Consequently, the relative velocity corresponds to the terminal velocity $v_{term}$ which can be evaluated as

$$v_{term} = \sqrt{\frac{2(m_{tot} - \rho_w V_w)g}{C_d \rho_w A_c}} \tag{3}$$

where $m_{tot} = 67.87\,\text{kg}$ is the total mass of the system and $A_c = 0.20\,\text{m}^2$ is the projected area of the container, whose shape can be approximated to the one of a sphere. Hence, the drag coefficient $C_d$ may be assumed as that of a sphere moving through a fluid ($C_d = 0.47$). The resulting sinking speed is $v_{term} = 28.24\,\text{mm/s}$, and it allows a progressive sinking, but slow enough to minimize the impact forces.

### 4.2 | FEM model for impact analysis

The critical phase of the container deposition is its impact against the seabed. Before analysing the consequences of the impact, it is necessary to define the stress state in the container wall due to the combined effect of the external seawater pressure and of the internal $CO_2$ pressure at the storage site, supposed to be at a depth of 2000 m. To this purpose, a 3D explicit dynamic analysis has been carried out using ABAQUS/Explicit. When containers are launched, the pressure of 10 MPa in the pipeline balances the internal pressure of 10 MPa due to $CO_2$. Once the containers are dropped, the external seawater pressure has been increased from 10 MPa to the final value of 20 MPa corresponding to the estimated seawater pressure at 2000 m depth, in a fictitious time of 0.0035 s. The volume reduction of the container is contrasted by the presence of the internal liquid $CO_2$ and sand, until a final equilibrium state is achieved. The container has been modelled by means of four-node conventional shell elements. In this element type, the mid-surface is taken as the reference surface on which engineering quantities are computed,[24,25,27] and consequently, its position has to be identified. Three regions of different thickness can be

**TABLE 4** Material density and volume

| Material | Density (kg/m$^3$) | Volume (m$^3$) |
|---|---|---|
| Glass | 2200 | $2.8894 \times 10^{-3}$ |
| Liquid $CO_2$ (10°C, 10 MPa) | 920.5 | $6.2558 \times 10^{-2}$ |
| Seawater (2000 m depth) | 1037 | — |

**TABLE 5** Liquefied $CO_2$ modelling parameters[30]

| | $\rho_{CO_2}$ (kg/m$^3$) | $C_0$ (m/s) | $\Gamma_0$ | $s$ | $\mu$ (MPa·s) |
|---|---|---|---|---|---|
| No sand | 920.50 | 563.50 | 0 | 0 | $9.7 \times 10^{-11}$ |
| With sand | 983.35 | 545.20 | 0 | 0 | $9.7 \times 10^{-11}$ |

distinguished in the container: 12 mm, 3.5 mm and a connection zone characterized by a smooth thickness variation. For simplicity, the plug has been considered as fixed to the container, so that one solid body can be analysed. The shell thickness in the 3D space is defined through an analytical field in the ABAQUS/CAE input.[28] The function to be introduced in the analytical field is given by Equation (4), with the reference system having origin in the centre of the spherical container:

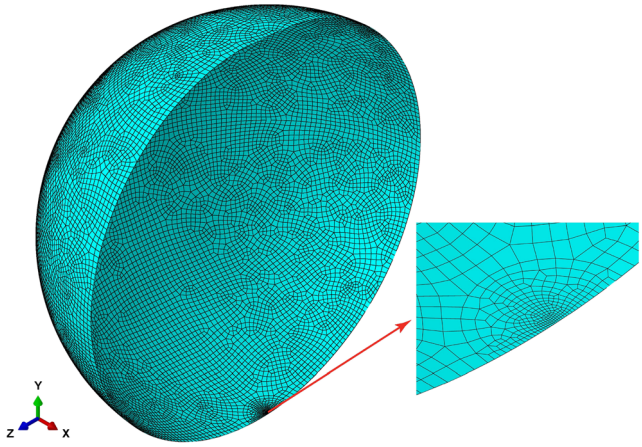


**FIGURE 8** Mesh adopted in the FEM model. A global size of 6 mm is used with a local refinement characterized by elements of 0.7 mm. Only one half of the model is depicted

$$y = \begin{aligned} &4.45\times10^{-11}(x^2+z^2)^{\frac{5}{2}} - 1.66\times10^{-8}(x^2+z^2)^2 + \\ &+2.99\times10^{-6}(x^2+z^2)^{\frac{3}{2}} + 0.11\times10^{-3}(x^2+z^2) + \\ &-0.13\times10^{-11}\sqrt{(x^2+z^2)} + 15.74 \end{aligned} \quad (4)$$

for $857\,\text{mm} \le x^2+z^2 \le 24292\,\text{mm}$.

A coupled fluid–solid analysis has been performed. The container has been modelled as a linear elastic homogeneous and isotropic body, while liquid carbon dioxide has been modelled with 3D solid elements according to the Mie–Grüneisen equation of state in the linear US–UP Hugoniot form.[29] In order to account for the contribution of the added sand, an equivalent $CO_2$ density and $C_0$, where $C_0$ is the sound speed in the fluid, have been evaluated without altering

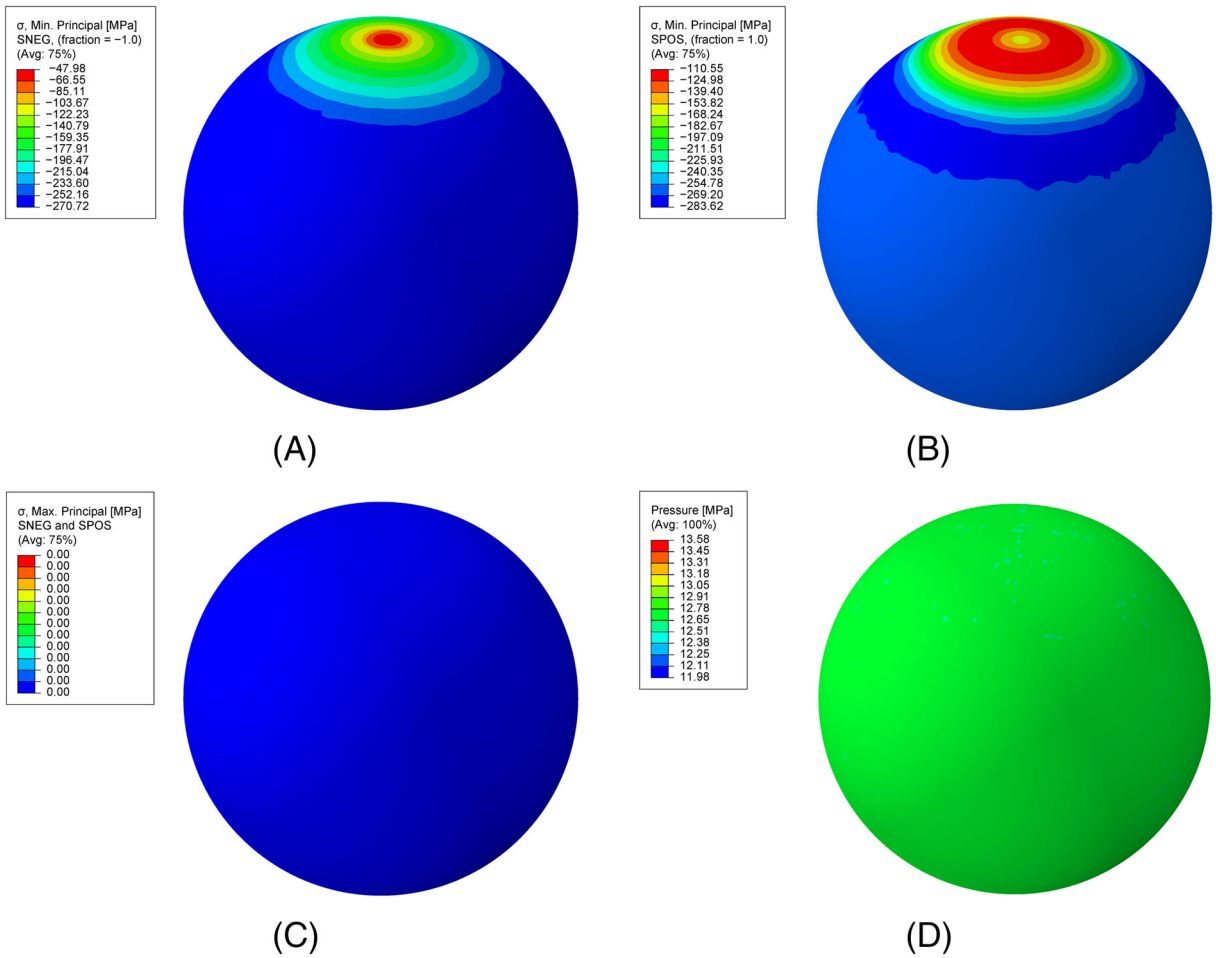


**FIGURE 9** Stresses caused by pressures at the storage site. (A) Minimum principal stresses on the internal surface SNEG. (B) Minimum principal stresses on the external surface SPOS. (C) Maximum principal stresses. (D) Pressure in $CO_2$

the liquid bulk modulus, which can be estimated as $K = C_0^2 \cdot \rho_{CO_2}$. The other required parameters are reported in Table 5 where $\Gamma_0$ and $s$ are Mie–Grüneisen parameters and $\mu$ is the fluid viscosity.

To establish the interaction between the container and the $CO_2$, a tie constraint has been applied between the two modelled parts. Global finite element size of 6 mm has been adopted in the model with a local refinement of 0.7 mm in correspondence of the estimated impact region of the container (see Figure 8). The finite element model is made of 26 805 four-node shell elements with reduced integration (S4R) for the container and 1 008 599 four-node linear tetrahedral elements (C3D4) for carbon dioxide. According to the result provided by ABAQUS/Explicit, the container is entirely compressed by the external seawater pressure. Moreover, due to the seawater pressure, an average increment of about 2.7 MPa in the internal $CO_2$ pressure is observed. The highest compressive stresses on the inner and outer surfaces are lower than the admissible ones; hence, the safety checks at this stage are fulfilled. The computed results are depicted in Figure 9.

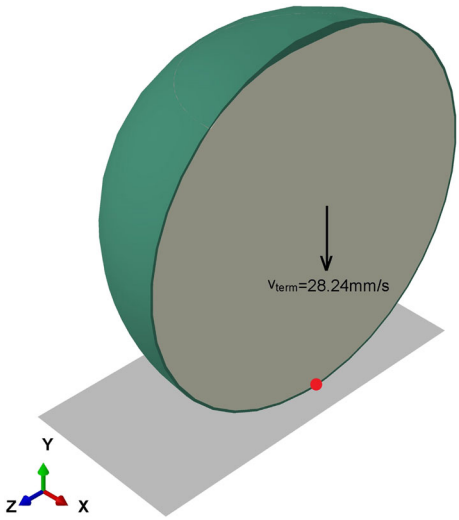


**FIGURE 10** Geometry of FEM model for the impact of a filled container against rigid soil. Red dot denotes first impact point. Only one half of the geometry is depicted

## 4.3 | Impact analysis

Two different falling scenarios have been analysed through 3D dynamic explicit analyses: (i) container impact against a rocky seabed and (ii) container impact against another container, already deposited onto the seabed. In both cases, maximum compressive and tensile principal stresses caused by the impact have been assessed and compared to their critical values. Since no accurate soil data are available, the modelling of seabed relies on the conservative assumption of a fixed rigid surface to simulate a rock-like soil. The same FEM model of the container described in Section 4.2 has been considered with the initial stress state estimated in the pre-impact phase. Furthermore, the terminal velocity has been applied to the mesh nodes of the full container in order to set the initial kinematic conditions of the body. Surface-to-surface interaction characterized by finite sliding and hard normal contact has been assumed to define the interaction properties between the container and the soil. The schematic model is shown in Figure 10.

During the impact, the most severe stresses arise in the lowest container point which first enters in contact with the soil. Therefore, the minimum principal stress variation of this point during the dynamic analysis has been monitored and plotted in Figure 11. The safety checks are fulfilled since the maximum compressive stress is lower than the admissible value. The container is entirely compressed by the water pressure during the impact phase, and tensile stresses do not arise during the impact.

Containers are supposed to remain stored on the seabed; hence, a launched container may hit an already deposited one. Finite element analyses have been performed also in this case. The schematic model is presented in Figure 12. Minimum principal stress variations in the lowest point of the two containers during the impact are reported in Figure 13. The safety is guaranteed since the peak values during impact are lower than the admissible values.

## 4.4 | Effects of geometrical dimensions

Thickness $t$ and diameter $D$ are geometric features playing a fundamental role, since they influence significantly the container structural

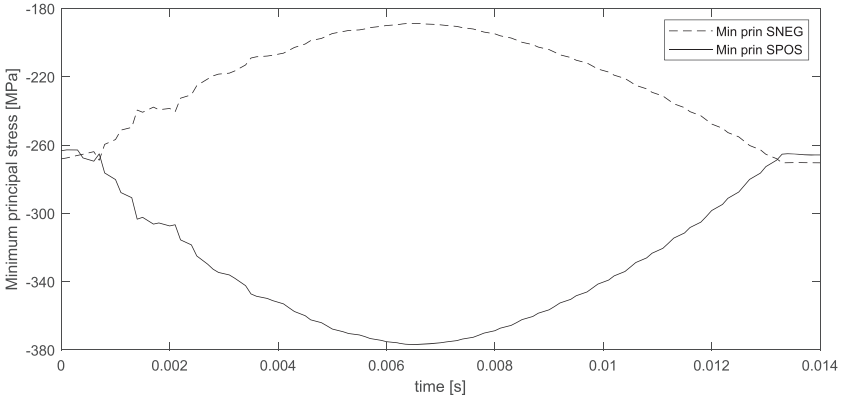


**FIGURE 11** Minimum principal stresses on the internal (SNEG) and external (SPOS) surface in the first contact point during the impact of a filled container with diameter 500 mm against rigid seabed

response.[31] Circumferential stresses under membrane regime for a spherical hollow vessel may be evaluated by

$$\sigma = \frac{PD}{4t} \quad (5)$$

where $P$ represents the applied pressure. However, the actual membrane stress level for a filled container is lower than that estimated by this formula, due to the stiffening effect provided by liquefied carbon dioxide in the container interior.

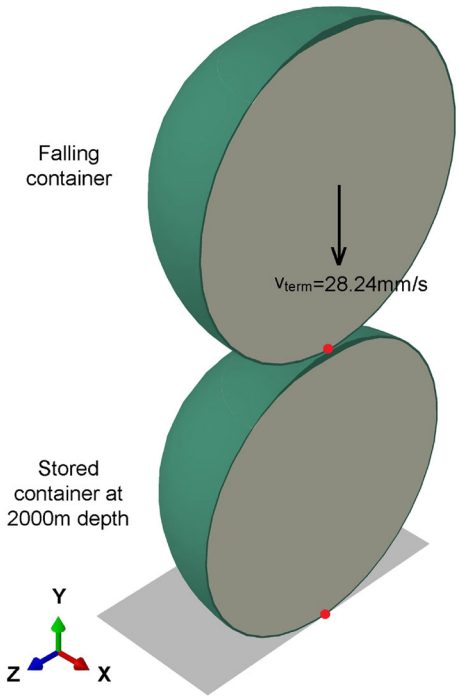


**FIGURE 12** Geometry of FEM model for the impact of a filled container against a stored container. Red dot denotes first impact point. Only one half of the geometry is depicted

Since the container diameter is an essential design parameter strictly related to the pipeline dimension, a different container diameter may be considered. In addition to the container with a diameter $D = 500$ mm considered so far, two more cases, characterized by a diameter of 300 mm with a thickness of 2.5 and 3 mm, have been analysed with ABAQUS/Explicit. In the first case (denoted by D300t2.5), a minimum amount of sand has been computed and introduced, while in the second case (denoted by D300t3), the shape has been calibrated in order to avoid sand. The masses and terminal velocities are summarized in Table 6, whereas the estimated minimum principal stresses during the impact against the rigid floor are reported in Figure 14 for both cases. The peak compressive principal stresses are lower than the admissible value; hence, the safety checks are fulfilled.

In the two analysed cases, the mass of liquefied $CO_2$ within each container is the same. However, the difference rests on the used quantity of glass. In the container D300t2.5, it is necessary to introduce 1.80 kg of sand, while in the container D300t3, no sand is required. It is worth noticing that the same material density has been assumed for sand and glass; hence, it is as if the quantity of sand was transformed in glass in the second case. The ratio between the mass of glass and mass of liquid $CO_2$ is 15.23% and 23.94% for the first and second cases, respectively, while a ratio of 11.61% was obtained for the $D = 500$ mm case. The estimated compressive stress state during the impact is less demanding in the container D300t3. Nevertheless, the choice of the container with sand may be more advantageous from the energetic and economic point of view due to the low cost and large availability of the raw material in the glass production phase.

**TABLE 6** Masses and terminal velocity in the two cases with containers of diameter 300 mm

| | $m_g$ (kg) | $m_{CO_2}$ (kg) | $m_g/m_{CO_2}$ (%) | $m_{sand}$ (kg) | $v_{term}$ (mm/s) |
|---|---|---|---|---|---|
| D300t2.5 | 1.80 | 11.82 | 15.23 | 1.04 | 34.11 |
| D300t3 | 2.83 | 11.82 | 23.96 | — | 30.13 |

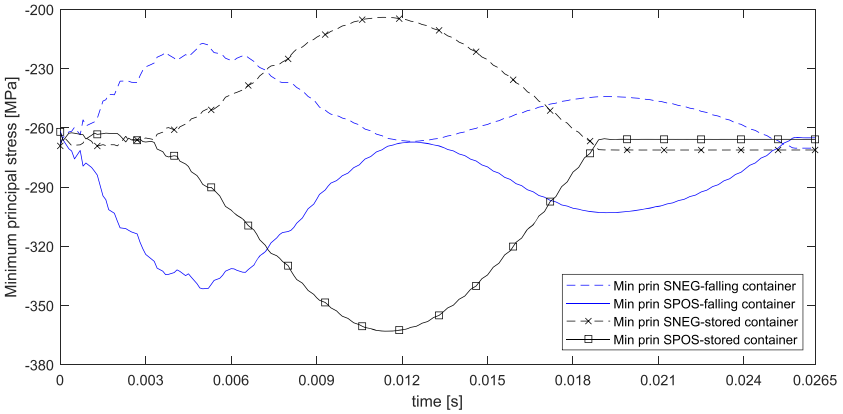


**FIGURE 13** Minimum principal stresses on the internal (SNEG) and external (SPOS) surface in the first contact points during the impact of a filled container with diameter 500 mm against a stored container

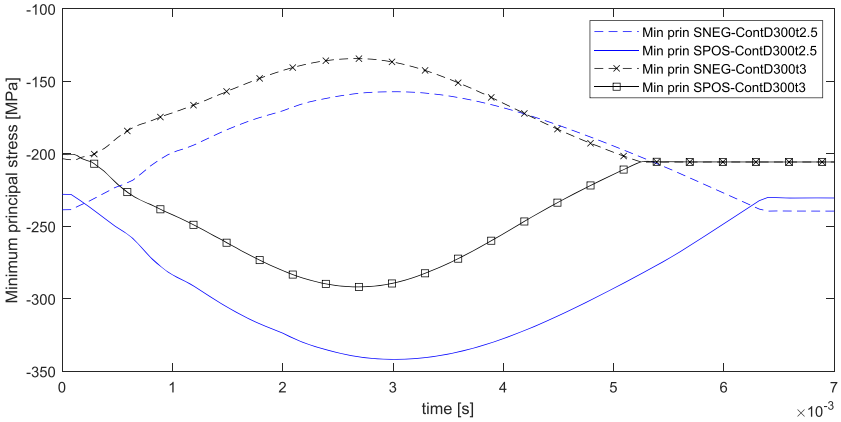


**FIGURE 14** Minimum principal stresses on the internal (SNEG) and external (SPOS) surface in the first contact point during the impact of containers with diameter 300 mm against the rigid soil

## 5 | CONCLUSIONS

The design of a glass container to meet the structural aspects of the CSCS technology has been performed. The container material and shape, which could be potentially adopted, have been defined through finite element analyses with ABAQUS/CAE. Borosilicate glass has been chosen to be the container material for its high compressive strength and chemical resistance in salty environment. However, glass is a brittle material due to the presence of defects that significantly limit its tensile resistance. Therefore, stress analyses have been carried out by ensuring both maximum and minimum principal stresses lower than the admissible stresses. Because of its structural efficiency, a thin spherical vessel has been chosen as an appropriate shape for the container. Due to the introduction of the plug required for the $CO_2$ filling, the container geometry has been modified and optimized. As a result, a stiffer and less material demanding container has been achieved. The optimized container hence is characterized by three portions with different thicknesses, ranging from 3.5 to 12 mm. In order to simulate the impact of the containers with the seabed, the zero-acceleration phase of the falling process has been considered for the evaluation of the terminal velocity. Once a container reaches the storage site at 2000 m depth, it is totally compressed by the seawater pressure. This represents a beneficial effect since it provides a precompression of the glass material preventing tensile stresses during impacts. Impact analyses of a container against rigid soil and against a stored container have been carried out. In both cases, safety checks were satisfied.

### ACKNOWLEDGEMENTS

The research was carried out within the Desarc-Maresanus project (www.desarc-maresanus.net), which received the financial support of Amundi SGR SpA. The authors thank Giovanni Cappello and Dennis Ross Morrey (CO2APPS) for their useful suggestions. Open Access Funding provided by Politecnico di Milano within the CRUI-CARE Agreement.

### DATA AVAILABILITY STATEMENT

Data are available on request from the authors.

### ORCID

*Cheng Fu* https://orcid.org/0000-0002-1326-6348

### REFERENCES

1. IPCC. Summary for policymakers. In: Global warming of 1.5 °C: an IPCC special report on the impacts of global warming of 1.5 °C above pre-industrial levels and related global greenhouse gas emission pathways, in the context of strengthening the global response to the threat of climate change, sustainable development, and efforts to eradicate poverty; 2018.
2. Fuss S, Lamb WF, Callaghan MW, et al. Negative emissions—part 2: costs, potentials and side effects. *Environ Res Lett*. 2018;13(6):63002.
3. Rockström J, Gaffney O, Rogelj J, Meinshausen M, Nakicenovic N, Schellnhuber HJ. A roadmap for rapid decarbonization. *Science*. 2017;355(6331):1269-1271.
4. IPCC. IPCC special report on carbon dioxide capture and storage. Prepared by Working Group III of the Intergovernmental Panel on Climate Change [Metz, B., O. Davidson, H. C. de Coninck, M. Loos, and L. A. Meyer (eds.)]; 2005.
5. OECD/IEA. 20 years of carbon capture and storage: accelerating future deployment. Technical report, Paris, International Energy Agency; 2016. www.iea.org/t/&c/
6. Nemet GF, Callaghan MW, Creutzig F, et al. Negative emissions—part 3: innovation and upscaling. *Environ Res Lett*. 2018;13(6):63003.
7. Aminu MD, Nabavi SA, Rochelle CA, Manovic V. A review of developments in carbon dioxide storage. *Applied Energy*. 2017;208:1389-1419. http://www.sciencedirect.com/science/article/pii/S0306261917313016
8. Global CCS Institute. Global status of CCS 2020. Technical report; 2020.
9. Dooley JJ. Estimating the supply and demand for deep geologic $CO_2$ storage capacity over the course of the 21st century: a meta-analysis of the literature. *Energy Proc*. 2013;37:5141-5150.
10. IPCC 2014. Climate change 2014: synthesis report. Contribution of Working Groups I, II and III to the Fifth Assessment Report of the Intergovernmental Panel on Climate Change.
11. Ajayi T, Gomes JS, Bera A. A review of $CO_2$ storage in geological formations emphasizing modeling, monitoring and capacity estimation approaches. *Petroleum Sci*. 2019;16(5):1028-1063.
12. Bui M, Adjiman CS, Bardow A, et al. Carbon capture and storage (CCS): the way forward. *Energy Environ Sci*. 2018;11(5):1062-1176.
13. Caserini S, Dolci G, Azzellino A, et al. Evaluation of a new technology for carbon dioxide submarine storage in glass capsules. *Int J Greenhouse Gas Control*. 2017;60:140-155. https://doi.org/10.1016/j.ijggc.2017.03.007

14. Barreto BB, Caserini S, Dolci G, Grosso M. Carbon dioxide submarine storage in glass containers: life cycle assessment and cost analysis of four case studies in the cement sector. *Mitigation Adapt Strat Global Change*. 2019;25(2):165-183.
15. Askeland DR, Phulé PP, Wright WJ, Bhattacharya DK. *The Science and Engineering of Materials*; Springer; 2003.
16. Werme L, Björner IK, Bart G, et al. Chemical corrosion of highly radioactive borosilicate nuclear waste glass under simulated repository conditions. *J Mater Res*. 1990;5(5):1130-1146.
17. Plodinec MJ. Borosilicate glasses for nuclear waste imobilisation. *Glass Technol*. 2000;41(6):186-192.
18. Bouras N, Madjoubi MA, Kolli M, Benterki S, Hamidouche M. Thermal and mechanical characterization of borosilicate glass. *Phys Proc*. 2009; 2(3):1135-1140.
19. Le Bourhis E. *Glass: Mechanics and Technology*: John Wiley & Sons; 2014.
20. Henderson J. *Ancient Glass: An Interdisciplinary Exploration*: Cambridge University Press; 2013.
21. Vogel W. *Glass Chemistry*: Springer Science & Business Media; 1994.
22. EN1748-1-1. Glass in building—special basic products—borosilicate glasses—part 1-1: definition and general physical and mechanical properties; 2004.
23. CNR-DT 210. Guide for the design, construction and control of buildings with structural glass elements; 2013.
24. Timoshenko SP. *Theory of Plates and Shells*, Vol. 148. McGraw-Hill; 1941.
25. Ventsel E, Krauthammer T. Thin plate and shells theory, analysis and applications; 2001.
26. Dassault Systèmes. Volume II: analysis. ABAQUS 614 Analysis User's Guide; 2014.
27. Dassault Systèmes. Volume IV: elements. ABAQUS 614 Analysis User's Guide; 2014.
28. Dassault Systèmes. ABAQUS/CAE user's guide; 2014.
29. Dassault Systèmes. Volume III: materials. ABAQUS 614 Analysis User's Guide; 2014.
30. Span R, Wagner W. A new equation of state for carbon dioxide covering the fluid region from the triple-point temperature to 1100 K at pressures up to 800 MPa. *J Phys Chem Ref Data*. 1996; 25(6):1509-1596.
31. Sundell HA, Mæs T. Relationship between impact energy and design parameters of glass bottles. *Packaging Technol Sci*. 1991;4(1):29-33. https://doi.org/10.1002/pts.2770040107

**How to cite this article:** Fu C, Cefis N, Cremonesi M, Perego U, Caserini S, Grosso M. Design of glass containers for submarine carbon storage. *Packag Technol Sci*. 2022;35(3): 259-271. doi:10.1002/pts.2624